Physics of Fluids

The rotation of two-dimensional elliptical porous particles in a simple shear flow with fluid inertia

Cite as: Phys. Fluids **32**, 043305 (2020); https://doi.org/10.1063/1.5145330
Submitted: 17 January 2020 . Accepted: 21 March 2020 . Published Online: 09 April 2020

Jiajia Liu (刘佳佳), **Chenggong Li** (李承功), **Mao Ye** (叶茂), **and Zhongmin Liu** (刘中民)

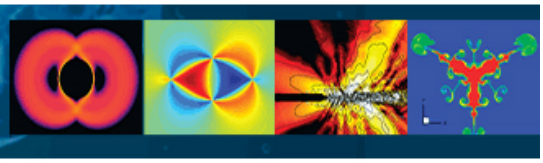

Physics of Fluids ARTICLE scitation.org/journal/phf

The rotation of two-dimensional elliptical porous particles in a simple shear flow with fluid inertia

Cite as: Phys. Fluids 32, 043305 (2020); doi: 10.1063/1.5145330
Submitted: 17 January 2020 • Accepted: 21 March 2020 •
Published Online: 9 April 2020

Jiajia Liu (刘佳佳),[1,2] Chenggong Li (李承功),[1] Mao Ye (叶茂),[1,a)] and Zhongmin Liu (刘中民)[1]

AFFILIATIONS

[1] Dalian National Laboratory for Clean Energy, National Engineering Laboratory for MTO, Dalian Institute of Chemical Physics, Chinese Academy of Sciences, Dalian 116023, Liaoning, China

[2] University of Chinese Academy of Sciences, Beijing 100049, China

[a)] **Author to whom correspondence should be addressed:** maoye@dicp.ac.cn

ABSTRACT

The motion of porous particles in fluid flow is of fundamental importance in both natural and industrial processes. Recent work shows that fluid inertia can essentially alter the rotation of spherical porous particles in a simple shear flow. In this contribution, we examined the influence of fluid inertia on the rotation of elliptical porous particles in shear flow by solving the volume-averaged macroscopic equations with a two-dimensional lattice Boltzmann model. It is confirmed that the Darcy number *Da* has only a minor effect on the rotation of elliptical porous particles if fluid inertia is neglected. At finite fluid inertia, the elliptical porous particles, however, manifested time-periodic rotation with a non-uniform angular rate. For particles with small to intermediate *Da*, the period of rotation increases with Reynolds number *Re* up to a critical Re_c above which the particle would stop rotating. It is shown that the maximum and minimum angular rates, as well as the inclination angle at which the particle has a minimum angular rate, are significantly affected by *Da*. A scaling law for the period of rotation initially proposed for solid impermeable particles can be extended to elliptical porous particles at finite fluid inertia. For a highly permeable ellipse, however, Re_c has not been observed, and thus, the scaling law breaks down. We calculated the relative viscosity and intrinsic viscosity for simple shear flow containing elliptical porous particles. A formula developed for suspensions with vanishing *Re* can also be extended to correlate the intrinsic viscosity to *Da* at finite *Re*.

I. INTRODUCTION

Particulate two-phase flows are widely encountered in natural and industrial processes.[1,2] Examples include the flocs in the sedimentation processes,[3] catalyst clusters in a fluidized bed reactor,[4] and capsules for various biochemical applications.[5] Among others, the rotational behaviors of suspended particles and the associated rheological properties are of fundamental importance in understanding and controlling these processes, which, however, have received little attention due to the lack of effective experimental and modeling methods. The early research studies on the rotation of suspended particles were mainly based on theoretical analysis. Jeffery[6] first used a quasi-steady approach to analyze the motion of a solid ellipsoid suspended in a simple shear flow under Stokes flow where the fluid inertia was totally neglected. He found that the ellipsoid would rotate periodically in the simple shear flow with the final rotational state relying on the initial conditions. Noting that the energy dissipation differs for various rotational states, Jeffery further calculated the shear viscosity of the suspensions containing an ellipsoid based on energy dissipation in which he showed the maximum and minimum intrinsic viscosities for suspensions of an ellipsoid with various ellipticities. Following Jeffery's pioneering work, Robertson and Acrivos[7] analyzed the rotation of a circular cylinder at low Reynolds number (*Re*) using the asymptotic expansion method and found that the stokes solution can be improved by this method through properly incorporating the first-order effects of inertia. Harper and Leal[8,9] extended the perturbation theory to study the dynamics behaviors of the dumb-bell shaped particle and

rod-like particle in a shear flow and showed that both of these particles preferred a periodic orbit. Recently, Einarsson *et al.*[10] derived an equation for the orientational dynamics of a spheroid suspended in a simple shear flow using the reciprocal theorem. These theoretical analyses, however, are confined to the rotation of particles suspended at low-Reynolds number flow.

The rapid development of direct numerical simulations (DNS) methods in the past decades stimulated considerable interest in understanding the effect of fluid inertia on the rotation of suspended particles in fluid flows. Feng and Joseph[11] studied the rotation of an ellipsoid in a simple shear flow by directly solving the Navier–Stokes equations with a finite element method and discussed the deviation of the particle motion from the analytical orbit[6] derived considering fluid inertia. Ding and Aidun[12] further investigated the effects of fluid inertia on the rotational behaviors of a single solid particle of circular and elliptical shapes in a simple shear flow by using a lattice Boltzmann method (LBM). They found that there is a transit from being rotary to stationary for ellipse and ellipsoid with the increase in fluid inertia and further proposed a scaling law to describe the relationship between rotation periods and *Re*. Zettner and Yoda[13] experimentally verified the results of the rotation of a circular cylinder observed by Ding and Aidun[12] by particle image velocimetry (PIV). Yu *et al.*[14] examined the effects of fluid inertia on the rotation of a spheroid in a simple shear flow for *Re* up to 256 by a distributed Lagrangian multiplier based on a fictitious domain method in which they proposed an empirical model to describe the rotation rate of the spheroid. Huang *et al.*[15] studied the rotation of a neutrally buoyant spheroid in a Couette flow by using a multi-relaxation-time lattice Boltzmann method for *Re* up to 700. They showed that there exists several new periodic steady modes for prolate spheroids, and both the initial orientation and fluid inertia affect the rotation of the spheroid. For the associated viscosity, they showed that the intrinsic viscosities of the suspensions containing prolate or oblate ellipsoids in log-rolling and tumbling modes are consistent with the results given by Jeffery.[6] Recently, Huang *et al.*[16] calculated the shear viscosity for suspensions of prolate or oblate spheroidal particles in a simple shear flow and found that there exists a specified *Re* at which the intrinsic viscosity changes from a linear to nonlinear dependence on *Re*. Mao and Alexeev[17] investigated the motion of a solid spheroid in a simple shear flow and found that fluid inertia and the particle aspect ratio also affect the particle motion. Huang *et al.*[18] further studied the effects of the particle aspect ratio on the motion of a neutrally buoyant elliptical particle in a simple shear flow in detail. More recently, Li *et al.*[19] investigated the rotational dynamics of an ellipsoidal particle in shear flows and concluded that the steady states can be regarded as a combination of those in uniform flow and Couette flow and characterized by the inclination angle.

The aforementioned studies exclusively focused on solid impermeable particles. However, in practice, particles with porous structures are frequently encountered.[3–5] Masoud *et al.*[20] derived an analytical solution based on the Brinkman equation for the rotation of a porous ellipsoid in a simple shear flow with *Re* close to zero and showed that the permeability has negligible effect on the rotation of porous particles. Actually, Darcy's law and the Brinkman equation have been employed commonly to study fluid flows through porous media.[21–24] However, both Darcy's law and the Brinkman equation are confined to the cases where the *Re* is sufficiently small because the nonlinear inertial term is neglected in these two models.[25] Wang *et al.*[26] developed volume-averaged macroscopic equations in terms of the intrinsic phase-average velocity to describe fluid flows inside and outside the porous media at finite *Re* by incorporating the inertial term. Li *et al.*[27] developed a LBM code based on volume-averaged macroscopic equations and investigated numerically the rotation of a circular porous particle in a simple shear flow with fluid inertia. Their results confirmed the conclusion of Masoud *et al.*[20] that the permeability has little effect on the rotation of porous particles at low *Re*. However, Li *et al.*[27] further showed that the influence of permeability cannot be neglected when the fluid inertia is not negligible and the angular rate decreases with the increase in fluid inertia.

Recently, following the work of Li *et al.*,[27] Xu *et al.*[28] studied the shear viscosity of suspensions containing spherical porous particles freely rotating in a simple shear flow with LBM and showed that the intrinsic viscosity of the dilute suspension increases with *Re* and decreases with permeability at low *Re*. Liu *et al.*[29] extended the work of Xu *et al.*[28] to relatively high solid volume fraction and investigated the viscosity of semi-dilute suspensions containing circular porous particles. Later on, Liu *et al.*[30] studied the shear viscosity of suspensions containing elliptical porous particles with different ellipticities at low *Re* and proposed a simple empirical formula to describe the relation between intrinsic viscosity and permeability. More recently, Rezaee and Sadeghy[31] investigated the settling behaviors of a two-dimensional (2D) elliptical porous particle in a narrow channel with a lattice Boltzmann simulation. However, the rotational behaviors could be more complicated for non-spherical porous particles in the presence of fluid inertia, and the shear viscosity of suspensions of non-spherical porous particles may change accordingly. The effects of permeability on the rotational behavior of non-spherical porous particles, as well as the associated shear viscosity of the suspensions, therefore deserve further study.

The objective of this work is twofold: (1) to investigate the rotational behaviors of a neutrally buoyant elliptical porous particle suspended in simple shear flow with fluid inertia and (2) to study the corresponding shear viscosity of the suspensions containing elliptical porous particles with the focus on the effects of permeability and fluid inertia. The volume-averaged macroscopic governing equations[26] are adopted to describe the fluid flow outside and inside the porous particle at finite *Re*, and a modified single relaxation time lattice Boltzmann model is employed to solve the macroscopic equations.

II. METHODS

A. Governing equations

In this work, a neutrally buoyant elliptical porous particle in a 2D simple shear flow at finite *Re* is considered. The aspect ratio of the elliptical porous particle is $A = a/b = 2$, 2.5, and 3, where $2a$ and $2b$ are the major and minor axis of the elliptical particle, respectively. The particle is initially placed in the geometric center of the rectangular channel with the direction of the major axis perpendicular to the shear flow direction. The width of the channel is W and the height is set as $H = 0.5$ W. The shear flow is driven by the two parallel flat bounding walls moving along the opposite directions with the same constant velocity U. Here, *Re* is the particle shear Reynolds

number defined as $Re = \Gamma d^2/\nu$, where $\Gamma(=2U/H)$ is the shear rate of the system, d is set as $2a$ following Ref. 32, and ν is the kinematic viscosity of fluid.

The volume-averaged macroscopic equations employed in this work are derived by averaging the microscopic equations at the pore scale over a representative elementary volume (REV). Note that the REV scale is much larger than the pore scale so that there are sufficient pores inside the REV for averaging and much smaller than the whole domain so that the derived macroscopic equations can be employed in the porous particles. The volume-averaged macroscopic equations in which both the transient term and the nonlinear inertial term are included are written in terms of the intrinsic phase averaged velocity,

$$\nabla \cdot \langle u_f \rangle^f = 0, \tag{1}$$

$$\rho_f \left[\frac{\partial \langle \boldsymbol{u}_f \rangle^f}{\partial t} + \langle u_f \rangle^f \cdot \nabla \langle \boldsymbol{u}_f \rangle^f \right] = -\nabla \langle p_f \rangle^f + \mu \nabla^2 \langle \boldsymbol{u}_f \rangle^f + \boldsymbol{F}_m, \tag{2}$$

where $\langle \boldsymbol{u}_f \rangle^f$ and $\langle p_f \rangle^f$ are the intrinsic phase averaged velocity and the pressure,[26] respectively, ρ_f is the fluid density, and μ is the fluid viscosity. The intrinsic phase average is defined by

$$\langle \psi_k \rangle^k = \frac{1}{V_k} \int_{V_k} \psi_k dV, \tag{3}$$

where V_k denotes the volume of the k-phase in the representative volume V and ψ_k is a quantity of the k-phase. Here, k refers to either f or s representing the fluid phase or particle phase. With translational velocity $\boldsymbol{U}_p$ and rotational velocity $\boldsymbol{w}_p$, the homogeneous and isotropic elliptical porous particle moves rigidly with velocity $\boldsymbol{u}_s = \boldsymbol{U}_p + \boldsymbol{w}_p \times (\boldsymbol{r} - \boldsymbol{R})$, where $\boldsymbol{r}$ is the position vector of nodes inside the particle and $\boldsymbol{R}$ is the position vector of the mass center. $\boldsymbol{U}_p$ and $\boldsymbol{w}_p$ remain unchanged after the intrinsic phase average because the porous particle moves with a rigid-body motion. For simplicity, the intrinsic phase averaged velocity of particle phase $\langle \boldsymbol{u}_s \rangle^s$ is denoted by $\boldsymbol{V}_p$ in the following. Therefore $\langle \boldsymbol{u}_s \rangle^s = \boldsymbol{V_p} = \boldsymbol{U_p} + \boldsymbol{w_p} \times (\boldsymbol{r} - \boldsymbol{R})$ holds for the particle. $\boldsymbol{F}_m$ represents a sum of forces that can be given by

$$\boldsymbol{F}_m = -\frac{\varepsilon\mu}{K}\left(\langle \boldsymbol{u}_f \rangle^f - \boldsymbol{V}_p\right) - \rho_f \frac{\varepsilon^2 \boldsymbol{F}_\varepsilon}{\sqrt{K}}\left(\langle \boldsymbol{u}_f \rangle^f - \boldsymbol{V}_p\right)\left|\langle \boldsymbol{u}_f \rangle^f - \boldsymbol{V}_p\right| + \boldsymbol{G} \tag{4}$$

in which the first two terms are the linear and nonlinear interfacial forces exerted on the interface between fluid and the particle, respectively, and $\boldsymbol{G}$ is the gravitational force. The porosity of the particle ε is 0 when the porous particle reduces to a solid impermeable particle and approaches 1 if the volume of particle is fully filled with fluid. The porosity is set to be 1 when the volume-averaged macroscopic equations are used to formulate the pure fluid outside the porous particle. The permeability of the porous particle K is used to quantify the ability of porous particles to transmit fluid. The porous structure of the particle is depicted by the Darcy number (Da), which is the dimensionless permeability expressed as $Da = K/D^2$, where D refers to the characteristic length of the porous particle and takes the value of $2ab$. F_ε stands for the geometric function, which follows Ergun's correlation,[33] $F_\varepsilon = 1.75/\sqrt{150\varepsilon^3}$. In this work, for simplicity, the permeability K is associated with porosity ε via $K = \varepsilon^3 d_p^2/[150(1-\varepsilon)^2]$, where d_p is the characteristic diameter of the filling grains within the porous medium which takes the value of 100 μm.[34] The translational and rotational behaviors of the particles are governed by

$$\boldsymbol{F}_p = M_p \frac{d\boldsymbol{U}_p}{dt}, \tag{5}$$

$$\boldsymbol{T}_p = I_p \frac{d\boldsymbol{w}_p}{dt}, \tag{6}$$

where M_p is the particle mass, I_p is the moment of inertia of the particle, $\boldsymbol{F}_p$ and $\boldsymbol{T}_p$ are the net force and torque exerted on the porous particle, respectively.

B. The numerical method

The lattice Boltzmann model is employed to solve the volume-averaged macroscopic equations due to its accuracy and natural parallelism for simulating complex particle flows.[35,36] The corresponding lattice Boltzmann evolution equation of the density distribution function can be given as

$$f_\alpha(\boldsymbol{x} + \boldsymbol{e}_\alpha \delta_t, t + \delta_t) - f_\alpha(\boldsymbol{x}, t) = -\frac{1}{\tau}\left[f_\alpha(\boldsymbol{x}, t) - f_\alpha^{eq}(\boldsymbol{x}, t)\right] + \delta_t F_\alpha(\boldsymbol{x}, t), \tag{7}$$

where $f_\alpha(\boldsymbol{x},t)$ is the particle distribution function (PDF) at position $\boldsymbol{x}$ at time t, $f_\alpha^{eq}(\boldsymbol{x}, t)$ is the equilibrium PDF, τ is the relaxation time, δ_t is the time step, and F_α is the force term in the α direction. The discrete velocity in α direction $\boldsymbol{e}_\alpha$ can be given as

$$\boldsymbol{e}_\alpha = \begin{cases} (0,0), & \alpha = 0 \\ c\left(\cos\left[(\alpha-1)\frac{\pi}{2}\right], \sin\left[(\alpha-1)\frac{\pi}{2}\right]\right), & \alpha = 1,2,3,4 \\ \sqrt{2}c\left(\cos\left[(2\alpha-1)\frac{\pi}{4}\right], \sin\left[(2\alpha-1)\frac{\pi}{4}\right]\right), & \alpha = 5,6,7,8, \end{cases} \tag{8}$$

where $c = \delta_x/\delta_t$ is the lattice speed with the lattice size δ_x. The force term in the α direction F_α is

$$F_\alpha = \rho_f \omega_\alpha \left(1 - \frac{1}{2\tau}\right)\left[\frac{\boldsymbol{e}_\alpha \cdot F_m}{c_s^2} + \frac{\boldsymbol{e}_\alpha . \boldsymbol{u}}{c_s^4}(\boldsymbol{e}_\alpha \cdot \boldsymbol{F}_m) - \frac{\boldsymbol{u} \cdot \boldsymbol{F}_m}{c_s^2}\right], \tag{9}$$

and the equilibrium PDF $f_\alpha^{eq}(\boldsymbol{x}, t)$ is defined as

$$f_\alpha^{eq}(\boldsymbol{x}, t) = \rho_f \omega_\alpha \left[1 + \frac{\boldsymbol{e}_\alpha \cdot \boldsymbol{u}}{c_s^2} + \frac{(\boldsymbol{e}_\alpha \cdot \boldsymbol{u})^2}{2c_s^4} - \frac{\boldsymbol{u}^2}{2c_s^2}\right], \tag{10}$$

where ω_α is the weight parameter given by $\omega_0 = 4/9$, $\omega_{1-4} = 1/9$, and $\omega_{5-8} = 1/36$, c_s is the lattice sound speed with $c_s^2 = 1/3$, and $\boldsymbol{u}$ is the intrinsic phase averaged velocity of the fluid phase $\langle \boldsymbol{u}_f \rangle^f$. The macroscopic properties are related to the PDF by

$$\rho_f = \sum_{\alpha=0}^{8} f_\alpha, \quad \rho_f \boldsymbol{u} = \sum_{\alpha=0}^{8} \boldsymbol{e}_\alpha f_\alpha + \frac{1}{2}\delta_t \rho_f \boldsymbol{F}_m. \tag{11}$$

By introducing Eq. (4) into Eq. (11), the velocity $\boldsymbol{u}$ can be calculated by

$$\boldsymbol{u} = \frac{\boldsymbol{v}}{d_0 + \sqrt{d_0^2 + d_1|\boldsymbol{v}|}} + \boldsymbol{V}_p, \tag{12}$$

where $\boldsymbol{v}$ denotes the temporal variable defined as

$$\rho \boldsymbol{v} = \sum_{\alpha=0}^{8} \boldsymbol{e}_\alpha f_\alpha + \frac{1}{2}\delta_t \rho \boldsymbol{G} - \rho \boldsymbol{V}_p. \tag{13}$$

The two parameters d_0 and d_1 can be respectively given by

$$d_0 = \frac{1}{2}\left(1 + \frac{1}{2}\delta_t \frac{\varepsilon \nu}{K}\right) \tag{14a}$$

and

$$d_1 = \frac{1}{2}\delta_t \frac{\varepsilon^2 F_\varepsilon}{\sqrt{K}}. \tag{14b}$$

For the simple shear flow in this work, the periodic boundary conditions are applied in the flow direction and non-equilibrium bounce-back schemes[37] are implemented to account for the two moving impermeable bounding walls. It should be noted that no explicit boundary conditions are required for the interface between the porous particle and fluid because a second order viscous term is already included in the macroscopic conservation equations.

The momentum-exchange method[38] is used to calculate the drag force and torque exerted by fluid on particles because of the numerical accuracy and easy implementation. In the momentum-exchange method, the force exerted on the particle is due to the momentum exchange between the external fluid nodes $\boldsymbol{x}_f = \boldsymbol{x}_b + \boldsymbol{e}_{\bar{\alpha}}\delta t$ and the internal boundary nodes $\boldsymbol{x}_b$, where $\boldsymbol{e}_{\bar{\alpha}}$ is the velocity in the opposite direction of $\boldsymbol{e}_\alpha$ with $\boldsymbol{e}_{\bar{\alpha}} = -\boldsymbol{e}_\alpha$. The momentum $\boldsymbol{e}_\alpha f_\alpha$ goes into the particle and contributes a momentum increment to it, and in the reverse direction, $\boldsymbol{e}_{\bar{\alpha}} f_{\bar{\alpha}} = -\boldsymbol{e}_\alpha f_{\bar{\alpha}}$ goes out of the particle and contributes a momentum decrement to it. Therefore, even though the momentum-exchange method was presented for the solid bodies, it can be adopted to calculate exactly the force and torque on the porous particle. The drag force $\boldsymbol{F}_p$ and torque $\boldsymbol{T}_p$ can be expressed as

$$\boldsymbol{F}_p = \sum_{all x_b} \sum_{\alpha \neq 0} \boldsymbol{e}_\alpha \left[f_\alpha(\boldsymbol{x}_b, t) + f_{\bar{\alpha}}(\boldsymbol{x}_b + \boldsymbol{e}_{\bar{\alpha}}\delta_t, t)\right] \times \left[1 - w(\boldsymbol{x}_b + \boldsymbol{e}_{\bar{\alpha}}\delta_t)\right] \tag{15}$$

and

$$\boldsymbol{T}_p = \sum_{all x_b} \sum_{\alpha \neq 0} (\boldsymbol{x}_b - \boldsymbol{R}) \times \left[\boldsymbol{e}_\alpha \left[f_\alpha(\boldsymbol{x}_b, t) + f_{\bar{\alpha}}(\boldsymbol{x}_b + \boldsymbol{e}_{\bar{\alpha}}\delta_t, t)\right] \times \left[1 - w(\boldsymbol{x}_b + \boldsymbol{e}_{\bar{\alpha}}\delta_t)\right]\right]. \tag{16}$$

Here, $w(i,j)$ is a scalar array where a value of 0 is assigned for those lattice sites (i,j) occupied by fluid and a value of 1 is assigned for lattice nodes inside the particle.

For an elliptical neutrally buoyant particle in a simple shear flow, the relative viscosity can be calculated based on energy dissipation of the flow system,[16]

$$\eta_r = \frac{\mu^*}{\mu} = \frac{\langle \bar{\sigma} \rangle}{\rho_f \nu \Gamma}, \tag{17}$$

where μ^* is the effective viscosity of particle suspensions, μ is the viscosity of the corresponding pure fluid, and $\langle \bar{\sigma} \rangle$ is spatially and temporally averaged shear stress. To calculate η_r, first, the shear stress σ can be obtained by the second-order moments of the distribution function,

$$\sigma(\mathrm{x}) = -\left(1 - \frac{1}{2\tau}\right) \sum f_\alpha^{neq} \boldsymbol{e}_{\alpha x} \boldsymbol{e}_{\alpha y}, \tag{18}$$

where $f_\alpha^{neq} = f_\alpha - f_\alpha^{eq}$ is the non-equilibrium PDF and $\boldsymbol{e}_{\alpha x}$ and $\boldsymbol{e}_{\alpha y}$ stand for the x- and y-components of $\boldsymbol{e}_\alpha$, respectively. The shear stress exerted on the fluid nodes that are nearest to the wall nodes is equal to that exerted on the moving flat walls. The drag force acting on the two flat bounding walls can be obtained by integrating the shear stress over the flat walls. Therefore, we can obtain the spatially averaged shear stress by dividing the drag force by the area of the moving bounding walls. Then, $\langle \bar{\sigma} \rangle$ is obtained by further averaging shear stress over time.[15]

III. MODEL VALIDATION

In this section, we validate the numerical model by considering three testing cases: fixed elliptical porous particle in simple shear flow and rotation of an elliptical particle in a simple shear flow at small and at finite Re. In this section, we fixed the aspect ratio of the elliptical particle. The major and minor axis of the elliptical porous particle are set to be $2a = 0.16$ cm and $2b = 0.08$ cm, respectively. Besides, the width of the rectangular channel is set equal to $W = 3.2$ cm and the height $H = 1.6$ cm. After checking the grid independence of our model, 360 lattices are used to resolve 1 cm.

We first investigate the torque acting on the fixed elliptical porous particle by the fluid in a simple shear flow at $Re = 0.08$. In this validation case, the elliptical porous particle is fixed in the geometric center of the channel; therefore, Eq. (5) breaks down. According to Masoud *et al.*,[20] the analytical solution of the torque acting on the porous particle can be given by

$$T = 2\pi\mu\Gamma a^2 \frac{I_2(\beta)}{I_0(\beta)}. \tag{19}$$

In Eq. (19), β is defined as $\beta = \sqrt{ab/K}$ and I_0 and I_2 are both modified Bessel functions of the first kind. The dimensionless torque $T/2\pi\mu\Gamma a^2$ is shown in Fig. 1 as a function of β. Here, β ranges from

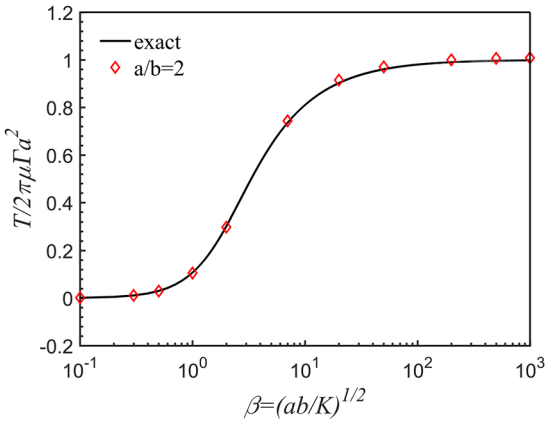

FIG. 1. Dimensionless torque $T/2\pi\mu\Gamma a^2$ acting on the fixed elliptical porous particle as a function of β.

10^{-1} to 10^{3}, and thus, the data range of Da is 2.5×10^{-7}–25, fully covering the data range of Da (10^{-6}–10^{-1}) investigated in this work. As can be seen in Fig. 1, our simulation results of torque acting on the particle agree well with the analytical solutions, which validates that the implementation of permeability is successful.

We then examined the rotational behavior of the elliptical particle suspended in the simple shear flow at Re ranging from 0.08 to 30. In the following two validation tests, Da is set to be extremely small, i.e., $Da = 2 \times 10^{-10}$, which means that the particle can be approximately treated as a solid impermeable particle. At vanishing Re where the effects of fluid inertia can be neglected, i.e., $Re = 0.08$, the analytical solutions of angle χ and angular rate $\dot{\chi}$ of the elliptical particle in shear flow were derived by Jeffery,[6]

$$\chi = tan^{-1}\left(\frac{a}{b}tan\frac{ab\Gamma t}{a^2+b^2}\right), \tag{20}$$

$$\dot{\chi} = \frac{\Gamma}{a^2+b^2}(a^2\cos^2\chi + b^2\sin^2\chi). \tag{21}$$

The comparisons of dimensionless angle χ/π and angular rate $\dot{\chi}/\Gamma$ obtained by simulations with the analytical solutions are shown in Fig. 2 for $Re = 0.08$. It can be seen that $\dot{\chi}/\Gamma$ changes periodically with the increase in dimensionless time Γt and χ/π tends to increase monotonously with Γt. As can be seen, both χ/π and $\dot{\chi}/\Gamma$ are in accordance with the analytical solutions developed by Jeffery.[6]

At finite Re where the inertia effects cannot be neglected, the elliptical particle manifests different rotational behaviors. The simulated angular rates of the elliptical particle vs dimensionless time are shown in Fig. 3 for Re = 0.08, 15, 28, and 30. The simulated angular rates are compared to the corresponding results by Ding and Aidun,[12] where the latter results are denoted by scatters in Fig. 3. As can be seen, for $Re \le 28$, the ellipse rotates periodically with a varying angular rate as Re changes. The increment of Re can lead to an extended rotation period of the elliptical particle. However, for $Re \ge 30$, the elliptical particle stops rotating and stays at a stationary position in the simple shear flow. Our simulation results of the angular rates at finite Re agree well with those of Ding and Aidun.[12]

We further calculate the rotation period ΓT of the elliptical particle at various Re, which is shown in Fig. 4. As can be seen, ΓT of the elliptical particle increases rapidly with Re. According to Ding and Aidun,[12] there exists a relation between the dimensionless rotation period ΓT and Re for the solid impermeable elliptical particle,

$$\Gamma T = C(Re_c - Re)^{-1/2}, \tag{22}$$

where C is a positive constant and Re_c is the critical Reynolds number above which the ellipse would stop rotating. For the solid impermeable elliptical particle,[12] C and Re_c are 100 and 29, respectively. As illustrated in Fig. 4, we can also correlate ΓT with Re via Eq. (22),

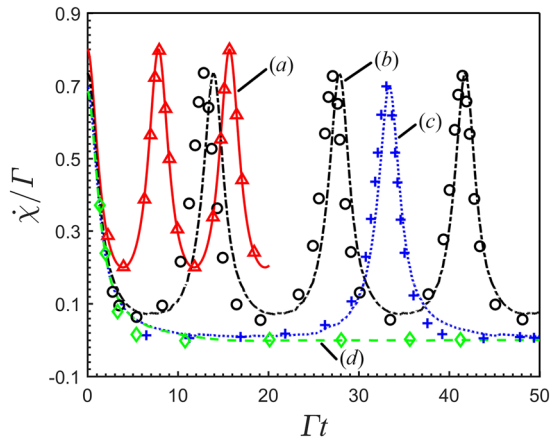

FIG. 3. Dimensionless angular rates $\dot{\chi}/\Gamma$ of the elliptical particle rotating in a simple shear flow as a function of dimensionless time Γt at (a) Re = 0.08, (b) Re = 15, (c) Re = 28, and (d) Re = 30. The lines are our simulation results, and scatters denote results by Ding and Aidun.[12]

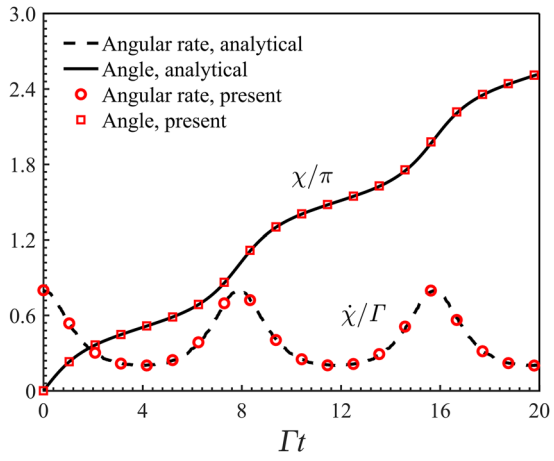

FIG. 2. Dimensionless angle χ/π and angular rate $\dot{\chi}/\Gamma$ of the elliptical particle rotating in the simple shear flow at Re = 0.08 and $Da = 2 \times 10^{-10}$ as a function of dimensionless time Γt.

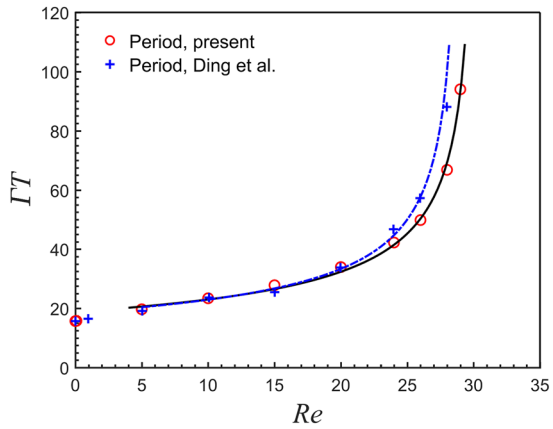

FIG. 4. Dimensionless rotation period ΓT of the elliptical particle as a function of Reynolds number Re.

where the best fits are obtained at $C = 103$ and $Re_c = 30$ with the least square method. It can be found that the best fits of C and Re_c by our simulation results are consistent with those reported by Ding and Aidun,[12] which further confirms that our model can well predict the rotational behavior of the elliptical particle in a simple shear flow at finite Re.

IV. RESULTS AND DISCUSSION

A. The rotation of elliptical porous particles in simple shear flow

In this section, we investigate the rotational behaviors of an elliptical porous particle freely rotating in a simple shear flow with fluid inertia taken into account. Specifically, we focus on $Da = 10^{-6}$–10^{-1} and $Re = 0.08$–60. The elliptical porous particle is initially placed at the geometric center of the rectangular channel with zero velocity, and there are no constraints on the motion of this particle. The minor axis of the elliptical porous particle is set to be $2b = 0.08$ cm, and the aspect ratio (AR) is defined as a/b and takes the values of 2, 2.5, and 3. In order to keep the confinement effect the same for different aspect ratios, we set the height of the rectangular channel to ten times the major axis (i.e., $H = 20a$), and the width W to $2H$. In the following, the aspect ratio refers to 2 unless otherwise stated. Our results show that the center of the porous particle remains at the initial position in all simulations. This means that the geometric center of the channel is also the equilibrium position of the elliptical porous particle initially placed at the center. Actually, it was shown that for 2D neutrally buoyant solid ellipse initially placed at the middle between two parallel bounding walls, the equilibrium position in the simple shear flow is also the centerline between the two walls.[18] It should be stressed, however, that here, we consider an ideal situation where neutrally buoyant particles initially placed at the center of the channel. These particles, although free to move, essentially stay at the equilibrium position and are ideal for studying the effects of fluid inertia and permeability on the rotation of porous particles.

First, the dimensionless angular rates $\dot{\chi}/\Gamma$ of the elliptical porous particle were calculated. Figure 5 shows the dimensionless angular rates $\dot{\chi}/\Gamma$ as a function of the dimensionless time Γt for $Da = 10^{-5}$, 10^{-2}, and 10^{-1}. In the case of $Da = 10^{-5}$ and 10^{-2}, as illustrated in Figs. 5(a) and 5(b), the elliptical porous particle demonstrates the time-periodic rotation with angular rates dependent upon Re. Especially, above a certain Re, the angular rate can decrease to 0 after a short time, indicating that the elliptical porous particle could stop rotating in the simple shear flow. The reason that the particle could stop rotating in a simple shear flow is closely related to the balance of torques exerted by the parallel bounding walls moving in opposite directions and the recirculating flow in the middle of channel, respectively, which we will discuss further later in this work. Therefore, for these elliptical porous particles, there similarly exists a critical Reynolds number Re_c above which the particle would eventually stop rotating and take a stationary position. When Da is further increased to 10^{-1}, as can be seen in Fig. 5(c), Re_c will not exist in the specified situations we studied in the current work. In addition, Fig. 5 also shows that both the maximum and minimum angular rates of the elliptical porous particle decrease with Re and the period of rotation of the particle increases with Re. In fact, as can be

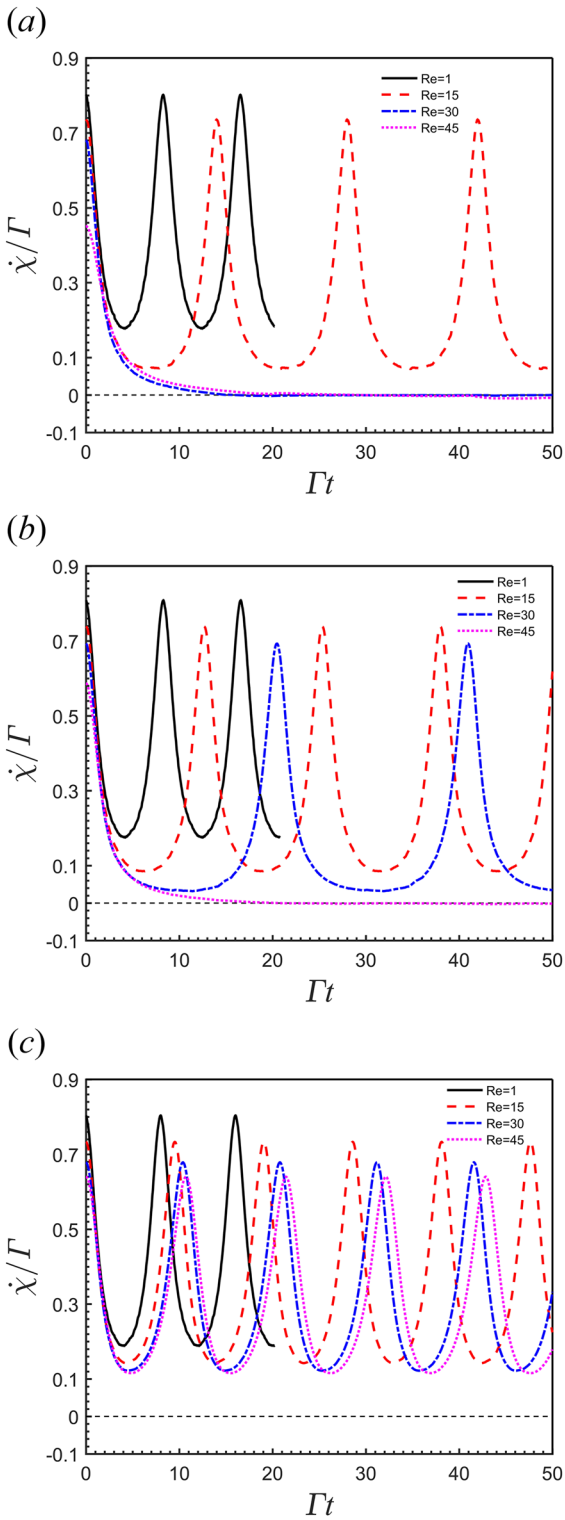

FIG. 5. Dimensionless angular rate $\dot{\chi}/\Gamma$ of the elliptical porous particle rotating in a simple shear flow as a function of dimensionless time Γt at $Re = 1$, 15, 30, and 45: (a) $Da = 10^{-5}$, (b) $Da = 10^{-2}$, and (c) $Da = 10^{-1}$.

evidenced by the rotation of a 3D solid spheroid with major or minor axis initially in the shear plane where the fluid inertia dominates the flow,[17] there is also a critical *Re* above which the spheroid would stop rotating and stay stationary. Both the maximum and minimum angular rates decrease with the increase in *Re*, leading to the increase in rotation period.[12,17,39] Apparently, the 3D solid spheroids with specified initial conditions in a simple shear flow behave very similarly to their 2D counterparts. In this sense, we argue that the 2D simulations results for porous spheroids might be a good starting point for understanding the motion of porous particles in fluid flow.

We further examine the effects of fluid inertia and permeability on the period of rotation of elliptical porous particles. Figure 6 shows the dimensionless periods ΓT as a function of *Re* for *Da* ranging from 10^{-6} to 10^{-1}. As can be seen, for $Re = 0.08$, ΓT are virtually the same for all *Da* studied, indicating that the permeability has little influence on the rotational behavior of the porous particle when the fluid inertia is negligible. This observation supports the conclusions by Masoud *et al.*[20] and Li *et al.*[27] With the further increase in *Re*, ΓT increases to various extents, dependent upon *Da* used. For small *Da* in the range of 10^{-6}–10^{-3}, ΓT shows a rapid increase with *Re* to infinity when *Re* reaches Re_c. The porous particle would eventually stop rotating when *Re* exceeds Re_c. Meantime, ΓT can be approximately approached by the results for solid impermeable particles reported by Ding and Aidun[12] and hardly affected by the change in *Da*. For intermediate *Da* in the range of 10^{-3}–2×10^{-2}, ΓT still shows a rapid increase with *Re* to infinity when *Re* reaches Re_c. The variation trend of ΓT with *Re* is also similar to that of 3D solid spheroids with specified initial conditions in a simple shear flow.[17,39] However, ΓT cannot be directly described by the results for the solid impermeable particle[12] as *Da* has essential effect on the rotational behavior of the elliptical porous particle. In this range of *Da*, the bigger the *Da*, the smaller the increasing rate of ΓT vs *Re*. For a highly permeable elliptical porous particle with $Da \geq 5 \times 10^{-2}$, ΓT increases slowly with *Re* and the Re_c has not been observed for this particle.

Based on the discussions above, we found that the scaling law $\Gamma T = C(Re_c - Re)^{-1/2}$ [Eq. (22)], which is initially proposed for the solid impermeable elliptical particle by Ding and Aidun,[12] might be extended to describe the relation between ΓT and *Re* for the elliptical porous particle. In Eq. (22), *C* and Re_c are two fitting parameters, where *C* is a positive constant and Re_c is the critical Reynolds number above which the porous particle would finally stop rotating. We fitted our simulation results with Eq. (22) and obtained *C* and Re_c for various *Da*, which are shown in Table I. In the meantime, based on the definition, we also derived the critical Reynolds number Re_{cr} using our simulation data, which is also included in Table I for comparison. Table I shows that Re_c and Re_{cr} are very close to each other for $Da \leq 2 \times 10^{-2}$, indicating that Eq. (22) can be reasonably used to describe the relation between the rotation period of the elliptical porous particle and *Re*. As can be seen in Table I, Re_c remains constant for small *Da* of 10^{-6}–10^{-3} and then increases with *Da* for intermediate *Da* of 10^{-3}–2×10^{-2}. It should be noted, however, that for $Da > 2 \times 10^{-2}$, the scaling law between ΓT and *Re* proposed by Ding and Aidun[12] breaks down due to the absence of Re_c.

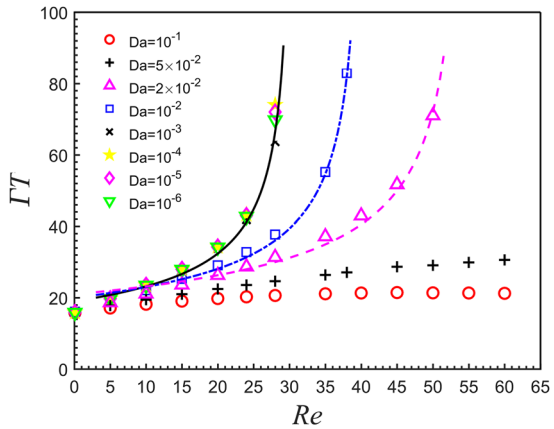

FIG. 6. Dimensionless rotation period ΓT of the elliptical porous particle as a function of *Re* at various *Da*.

In order to investigate whether there is a corresponding relationship between ΓT and *Re* for the porous ellipse with different aspect ratios and the effects of aspect ratio on the critical Reynolds number, the simulation results of the porous ellipse with the aspect ratio of 2.5 and 3 are shown in Fig. 7. As can be seen in Fig. 7, for particles with the aspect ratio of 2.5 and 3 and *Da* ranging from 10^{-6} to 2×10^{-2}, the relationship of ΓT and *Re* can be well fitted by Eq. (22), akin to the porous particles with an aspect ratio of 2. This suggests that the scaling law [Eq. (22)] is independent of the aspect ratio. Besides, the variation trends of dimensionless rotation period ΓT as a function of *Re* at various *Da* with the aspect ratio of 2.5 and 3 are similar to those of porous particles with an aspect ratio of 2, as discussed above. The fitting parameters *C* and Re_c in Eq. (22) together with the critical Reynolds number Re_{cr} obtained by our simulations for elliptical porous particles with the aspect ratio of 2.5 and 3 are shown in Tables II and III, respectively. As can be seen, for elliptical porous particles with the aspect ratio of 2.5 and 3, Re_c fitted with Eq. (22) is very close to Re_{cr} obtained from our simulations. This further shows that the scaling law [Eq. (22)] is independent of the aspect ratio. Moreover, for the elliptical porous particle with *Da* ranging from 10^{-6} to 2×10^{-2}, the critical Reynolds number decreases with the increase in aspect ratio. The variation trend of the critical Reynolds number with the aspect ratio is in accordance with those of the 2D solid ellipse[18] and the 3D solid ellipsoid with major or minor axis initially in the shear plane in a simple shear flow.[17]

To further understand the rotational behaviors of the elliptical porous particle in a simple shear flow, we also evaluated the effect of fluid inertia on the maximum and minimum angular rates

TABLE I. The fitting parameters for the scaling law shown in Eq. (22) [$\Gamma T = C(Re_c - Re)^{-1/2}$].

Da	2×10^{-2}	10^{-2}	10^{-3}	10^{-4}	10^{-5}	10^{-6}
C	154.85	128.20	106.75	104.33	104.62	105.07
Re_c	54.61	40.37	30.78	29.98	30.10	30.26
Re_{cr}	53	39	30	30	30	30

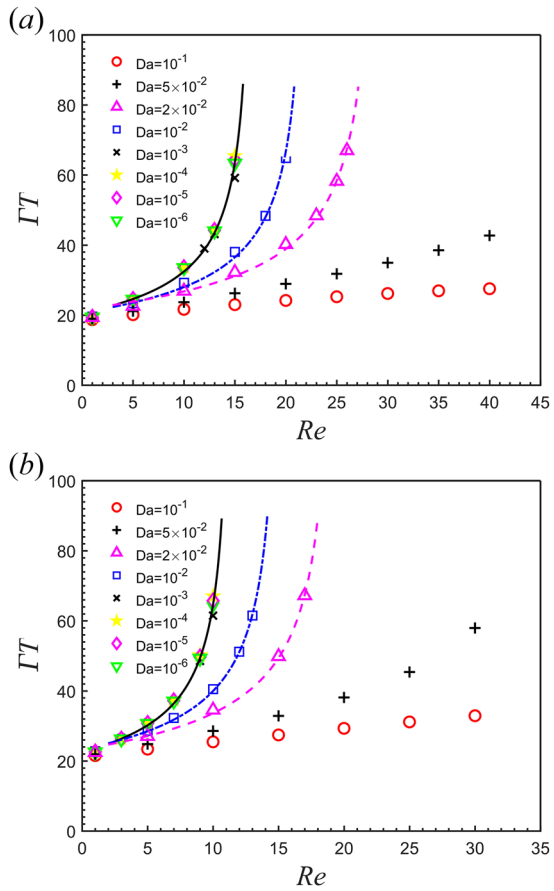

FIG. 7. Dimensionless rotation period ΓT of the elliptical porous particle as a function of *Re* at various *Da* with (a) an aspect ratio of 2.5 and (b) an aspect ratio of 3. The lines are obtained from fitting simulation data with Eq. (22).

of the elliptical porous particle with various *Da*. As demonstrated in Fig. 8(a), the maximum angular rate $\dot{\chi}_{max}/\Gamma$ decreases with *Re* for a *Da* of 10^{-6}–10^{-1}. As can be seen, the maximum angular rates are essentially overlapping for elliptical porous particles with varying *Da* at any given *Re* up to 20, meaning that permeability has a negligible effect on $\dot{\chi}_{max}/\Gamma$ with weak fluid inertia. With the further increase in *Re* from 20 to 60, a slight deviation of the maximum angular rates for particles with different *Da* can be observed, and the decreasing rate of $\dot{\chi}_{max}/\Gamma$ with *Re* becomes larger for particles with

TABLE II. The fitting parameters for the scaling law shown in Eq. (22) [$\Gamma T = C(Re_c - Re)^{-1/2}$] for particles with an aspect ratio of 2.5.

Da	2×10^{-2}	10^{-2}	10^{-3}	10^{-4}	10^{-5}	10^{-6}
C	116.60	97.56	84.53	84.29	84.23	84.36
Re_c	28.99	22.14	16.93	16.65	16.70	16.76
Re_{cr}	28	22	16	16	16	16

TABLE III. The fitting parameters for the scaling law shown in Eq. (22) [$\Gamma T = C(Re_c - Re)^{-1/2}$] for particles with an aspect ratio of 3.

Da	2×10^{-2}	10^{-2}	10^{-3}	10^{-4}	10^{-5}	10^{-6}
C	102.60	90.79	78.43	76.40	76.24	76.31
Re_c	19.32	15.16	11.62	11.30	11.34	11.39
Re_{cr}	19	15	11	11	11	11

higher *Da*. The minimum angular rate $\dot{\chi}_{min}/\Gamma$, as shown in Fig. 8(b), also decreases with the increase in *Re* for a *Da* of 10^{-6}–10^{-1}. For $Da = 10^{-6} - 2 \times 10^{-2}$, the elliptical porous particle would stop rotating and take a stationary orientation in the simple shear flow. In Fig. 8(b), a linear decrease in $\dot{\chi}_{min}/\Gamma$ down to 0 can be observed for the intermediate Reynolds number. The trend of $\dot{\chi}_{min}/\Gamma$ decaying with *Re* of elliptical porous particles is similar to its solid impermeable counterpart as reported by some researchers.[12,14] For $Da \geq 5 \times 10^{-2}$, the $\dot{\chi}_{min}/\Gamma$ shows a nonlinear decay with *Re*, and the decay rate gradually reduces and finally reaches an approximate plateau

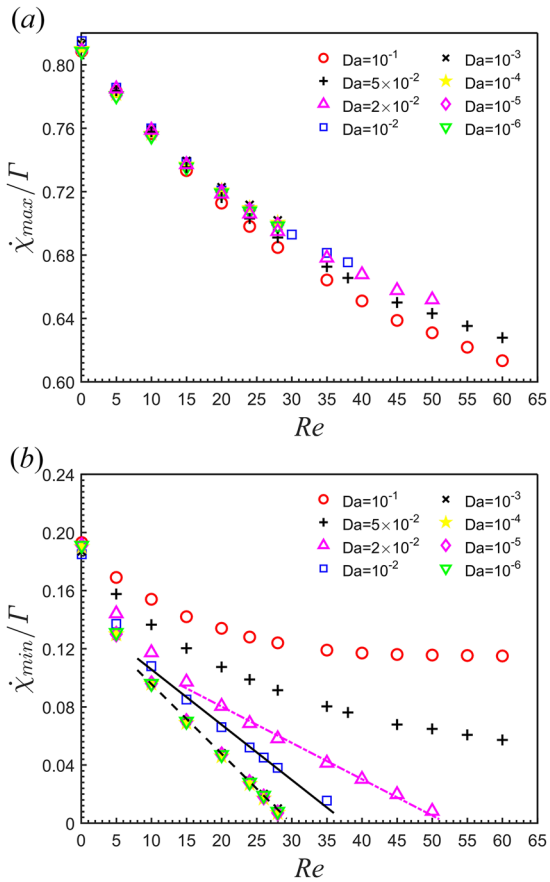

FIG. 8. The maximum angular rate $\dot{\chi}_{max}/\Gamma$ (a) and minimum angular rate $\dot{\chi}_{min}/\Gamma$ (b) of the elliptical porous particle as a function of *Re* at various *Da*.

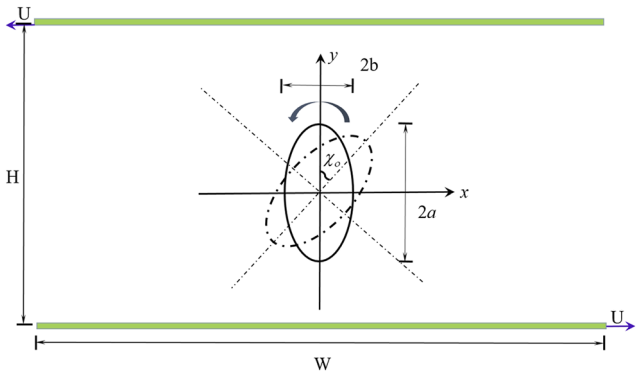

FIG. 9. The schematic diagram of the angle χ_o at which the porous ellipse has its minimum angular rate.

as *Re* increases. This indicates that highly permeable particles rotate faster than those of small permeability at the same *Re*. By extrapolation, it seems that those highly permeable elliptical particles may stop rotating in a simple shear flow at a much higher *Re*. This might be interesting for further exploration. The variation trends of maximum and minimum angular velocity of these elliptical porous particles are similar to those of 3D solid spheroids.[17,39]

The angle at which the porous ellipse has its minimum angular rate, which is denoted by A_{gm} in this work, is important for understanding the rotational behavior in shear flow. We studied the influences of fluid inertia and permeability of particles on A_{gm}. Note that A_{gm} refers to the angle between the major axis of the porous ellipse and the positive direction of the *y*-axis, as shown in Fig. 9. In Fig. 10, A_{gm}/π, i.e., the angle normalized by π, was reported for $Da = 2 \times 10^{-10}$–10^{-1} and $Re = 0.08$–60. The accurate values of A_{gm}/π in Fig. 10 are also given in Table IV. When the porous particle can be approximately treated as its solid impermeable counterpart with vanishing fluid inertia, i.e., $Da = 2 \times 10^{-10}$ and $Re = 0.08$, the normalized angle A_{gm}/π approaches 0.5. This means that the major axis

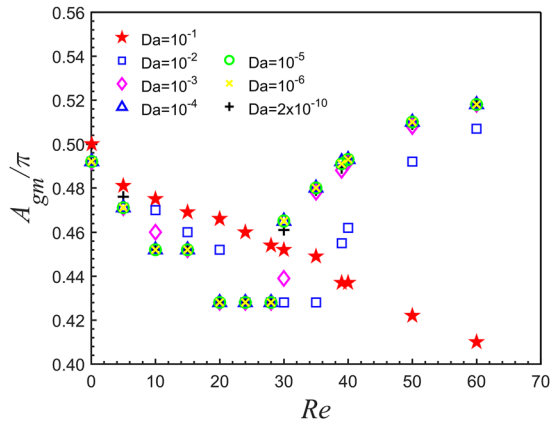

FIG. 10. The normalized angle corresponding to the minimum angular rate, A_{gm}/π, at various *Re* and *Da*.

of the elliptical particle becomes parallel to the shear direction when the porous ellipse has its minimum angular rate, which agrees well with the results by Ding and Aidun.[12] The angle decreases with the increase in *Re* when $Re < 28$, indicating that the major axis of the ellipse can get closer to the positive direction of the *y*-axis with enhanced fluid inertia when the ellipse has its minimum of the angular rate. This observation is in accordance with the results of solid elliptical particles reported by Ding and Aidun.[12] However, for $Re \geq Re_c$ ($Re_c = 30$), where the elliptical porous particles would finally stop rotating and take a stationary position in the simple shear flow, it is found that the inclination angle increased from 0.461π to 0.518π when *Re* varies from 30 to 60. This means that the major axis of the particle gets further away from the positive direction of the *y*-axis with the increase in fluid inertia when $Re \geq Re_c$. As for elliptical porous particles with $10^{-6} \leq Da \leq 10^{-2}$, the variations of the angle at which the ellipse has a minimum angular rate vs *Re* are similar to that with $Da = 2 \times 10^{-10}$, i.e., the case of solid impermeable particles. However, for highly permeable elliptical particles with $Da = 10^{-1}$, the angle decays monotonously with *Re* up to 60. From Fig. 10, it is also shown that when $Re < Re_c$, for small *Da* ranging from 10^{-6} to 10^{-4}, the angle decreases with *Re* at the almost same rate, whereas for intermediate to large *Da* ranging from 10^{-3} to 10^{-1}, the decreasing rate becomes smaller. Besides, we observed that the elliptical porous particle could rotate in the opposite direction for $Da \leq 10^{-2}$ at $Re = 60$ when it is about to stop rotating in a simple shear flow.

To qualitatively explain the behaviors of elliptical porous particles in a simple shear flow, we plotted the streamlines of the flow fields under various *Re* and *Da*. To clearly show the effects of *Re* and *Da* on the flow patterns, a fixed orientation angle of 0.23π is chosen for all porous particles in Fig. 11. As demonstrated in Fig. 11, the flow patterns are similar to those of solid impermeable particles.[12] For a solid particle freely rotating in a simple shear flow, it is argued that the shear flow adjacent to the two parallel bounding walls moving in opposite directions exerts a positive torque on the particle, whereas the recirculating flow in the middle of the channel has a negative contribution to the particle rotation. Besides, there is a third fluid layer near and around the particle surface, which transfers momentum from the shear layer and the recirculation region to the particle.[12,27] For porous particles, the third fluid layer near and around the particle plays an important role due to the penetration of fluid. As shown in Figs. 11(a)–11(c), for the elliptical porous particle with $Da = 10^{-2}$, the recirculation region is getting larger when *Re* increases, indicating that the negative torque exerted on the porous particle is enhanced by fluid inertia. Hence, the period of rotation of the elliptical porous particle increases and the minimum angular rate decreases with *Re*. When *Re* increases to Re_c, the negative torque exerted on the porous particle enhanced by fluid inertia balances the positive torque by shear flow. Thus, the porous particle is very likely to stop rotating. Furthermore, Figs. 11(d)–11(f) show that with the increase in *Da*, there are more streamlines penetrating through the elliptical porous particle and the recirculation region is getting smaller. The increased permeability of the elliptical porous particle can reduce the negative contribution of the recirculation region to the particle rotation. Consequently, the period of rotation decreases and the angular rate increases with *Da*, which is in accordance with our results aforementioned.

TABLE IV. The accurate values of the normalized angle corresponding to the minimum angular rate, A_{gm}/π, at various *Re* and *Da*.

Re	Da = 10^{-1}	Da = 10^{-2}	Da = 10^{-3}	Da = 10^{-4}	Da = 10^{-5}	Da = 10^{-6}	Da = 2×10^{-10}
0.08	0.500	0.492	0.492	0.492	0.492	0.492	0.500
5	0.481	0.471	0.471	0.471	0.471	0.471	0.476
10	0.475	0.470	0.460	0.452	0.452	0.452	0.452
15	0.469	0.460	0.452	0.452	0.452	0.452	0.452
20	0.466	0.452	0.428	0.428	0.428	0.428	0.428
24	0.460	0.428	0.428	0.428	0.428	0.428	0.428
28	0.454	0.428	0.428	0.428	0.428	0.428	0.428
30	0.452	0.428	0.439	0.465	0.465	0.465	0.461
35	0.449	0.428	0.478	0.480	0.480	0.480	0.479
39	0.437	0.455	0.488	0.492	0.491	0.491	0.489
40	0.437	0.462	0.492	0.493	0.493	0.493	0.493
50	0.422	0.492	0.508	0.510	0.510	0.510	0.509
60	0.410	0.507	0.518	0.518	0.518	0.518	0.518

B. The shear viscosity of suspensions containing an elliptical porous particle

In particulate two-phase flows, the rheological property of suspensions is commonly characterized by viscosity. Einstein[40] developed a simple mathematical formula $\eta_r = \mu^*/\mu_f = 1 + [\tilde{\eta}]\phi$ for dilute suspensions containing spherical particles, where ϕ is the solid volume fraction and $[\tilde{\eta}]$ is its intrinsic viscosity, which is 2 in 2D and 2.5 in 3D cases.[41] Following Einstein's formula, many efforts have been devoted to obtain the relative viscosity and intrinsic viscosity of different particle suspensions.[42–46]

In this work, we studied the effects of the fluid inertia on the relative viscosity η_r of suspensions containing elliptical porous particles with a *Da* of 10^{-6}–10^{-1}. A fixed solid volume fraction $\phi = 0.2\%$ is chosen. The results of this work showed that for elliptical porous particle with $10^{-6} \le Da \le 10^{-1}$, there exists a critical Re_c above which the elliptical porous particle would stop rotating. Therefore, note that Re_c should be no less than 30 in the current work, and we limited our study to *Re* = 0.08–28 where the particle would keep freely rotating in the simple shear flow.

As illustrated in Fig. 12(a), for $Da = 10^{-6}$–10^{-1}, the relative viscosity η_r increases with the increase in *Re*. However, for small $Da = 10^{-6}$–10^{-3}, the curves of η_r vs *Re*, approaching those of the solid impermeable particles, are nearly overlapping. This means that the permeability of the particle has little effects on the relative viscosity for small *Da*. For intermediate to high $Da = 10^{-3}$–10^{-1}, however, *Da* has an apparent impact on the relative viscosity. The bigger the *Da*, the smaller the relative viscosity of the system. Furthermore, from Fig. 12(b), we could clearly see that the relative viscosity remains nearly constant for $Da \le 10^{-4}$ and then decreases rapidly when *Da* exceeds 10^{-4}, regardless of *Re*. Besides, we also check the effects of the aspect ratio of the porous ellipse

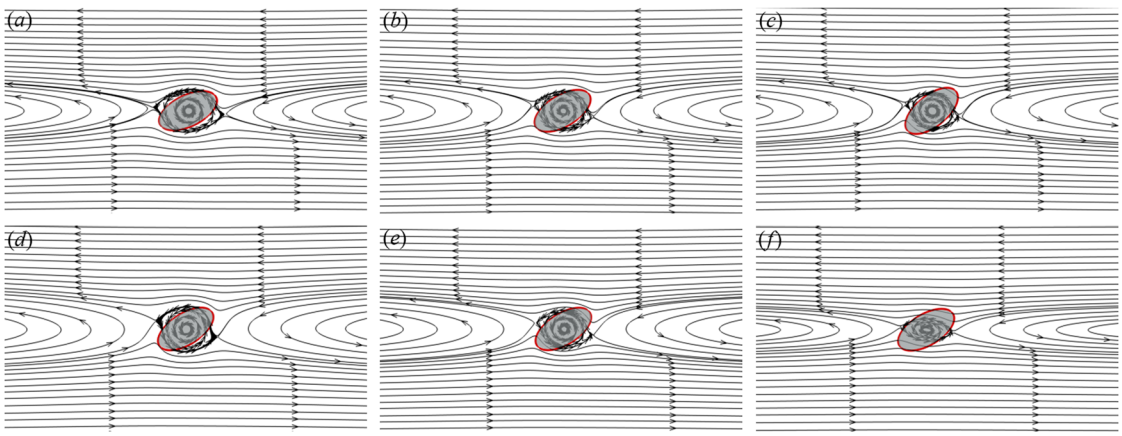

FIG. 11. Streamlines for simple shear flows past an elliptical porous particle at various *Re* and *Da*, [(a)–(c)] for $Da = 10^{-2}$ and [(d)–(f)] for *Re* = 28: (a) *Re* = 5, (b) *Re* = 20, (c) *Re* = 35, (d) $Da = 10^{-4}$, (e) $Da = 10^{-2}$, and (f) $Da = 10^{-1}$.

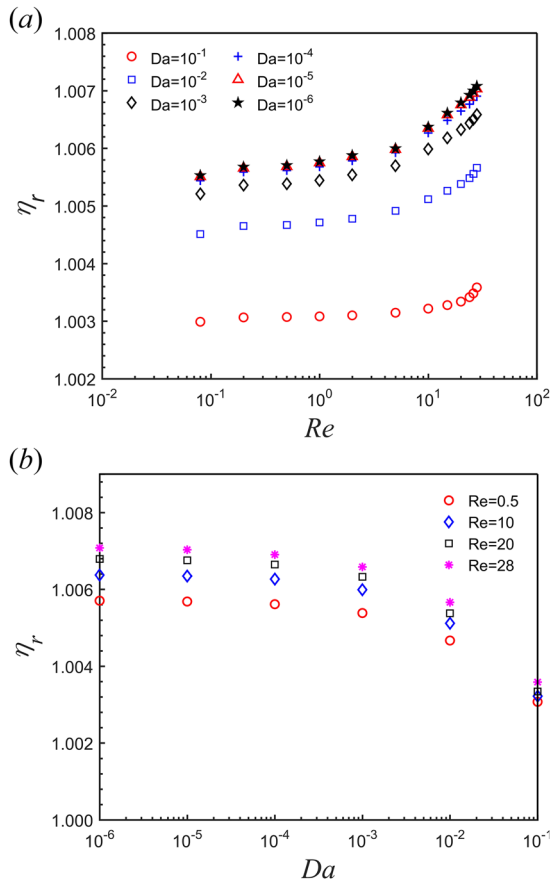

FIG. 12. The relative viscosity η_r (a) as a function of *Re* at various *Da* and (b) as a function of *Da* at various *Re*.

on the relative viscosity of suspensions. Results demonstrate that at $\phi = 0.5\%$ and $Re = 20$, for Da ranging from 10^{-6} to 10^{-1}, the relative viscosity of suspensions containing an elliptical porous particle increases with the increase in the aspect ratio (AR = 1, 2

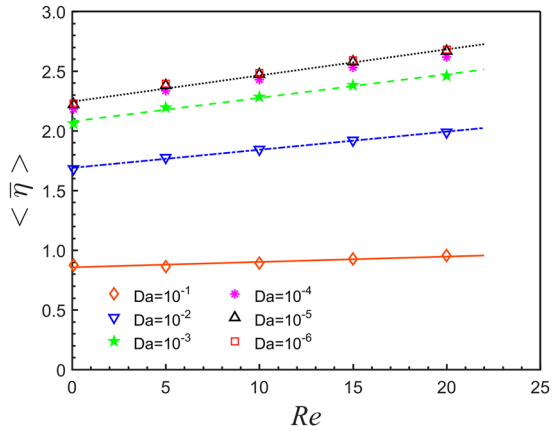

FIG. 13. The intrinsic viscosity $\langle\bar{\eta}\rangle$ as a function of *Re* at various *Da*.

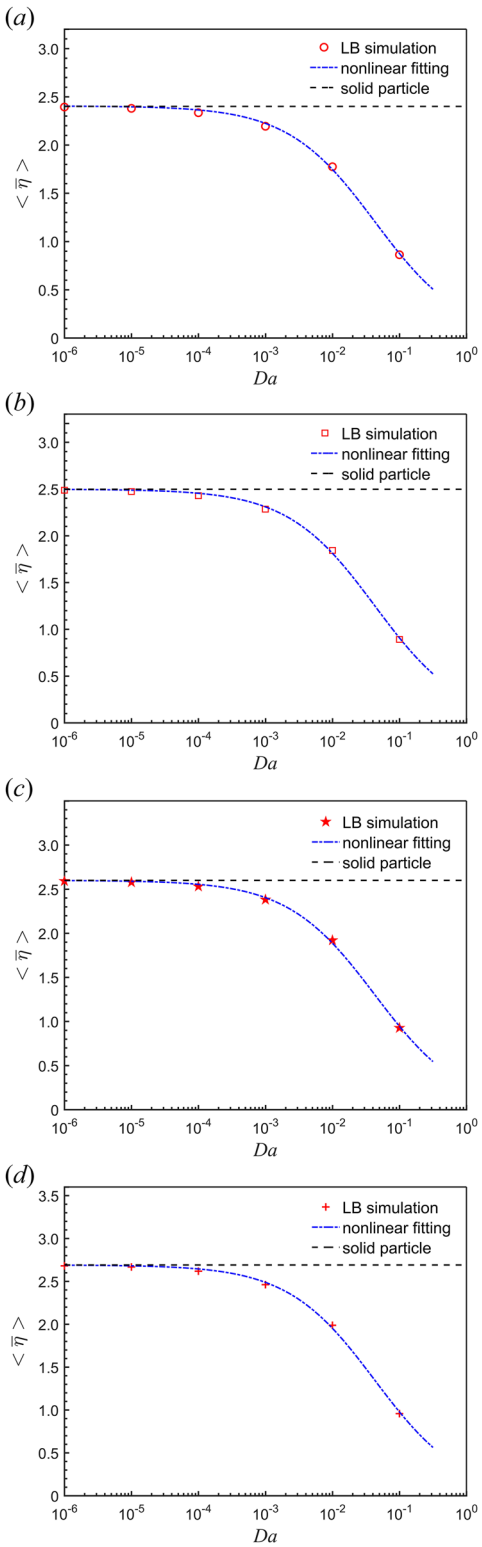

FIG. 14. The intrinsic viscosity $\langle\bar{\eta}\rangle$ as a function of *Da* at various *Re*: (a) *Re* = 5, (b) *Re* = 10, (c) *Re* = 15, and (d) *Re* = 20.

TABLE V. The fitting parameters for correlations in Eq. (23).

Parameters	$Re = 0.08$	$Re = 5$	$Re = 10$	$Re = 15$	$Re = 20$
m	2.26	2.40	2.50	2.60	2.69
n	7.47	8.11	8.13	8.12	8.14

and 4). This conclusion is similar to that at vanishing fluid inertia ($Re = 0.08$).[30]

We further checked the effects of fluid inertia on the intrinsic viscosity of the suspensions containing an elliptical porous particle. As shown in Einstein's formula, the intrinsic viscosity $[\tilde{\eta}]$ can be obtained by a linear fitting of the relative viscosity with the solid volume fraction.[40] The solid volume fraction ϕ ranging from 0.2% to 2% is considered here. As can be seen in Fig. 13, the intrinsic viscosity $[\tilde{\eta}]$ of the suspension containing an elliptical porous particle increases linearly with Re for all Da considered. The relations between intrinsic viscosity and Re at various Da are similar to those of suspensions containing a 3D tumbling ellipsoidal solid particle[16] in a simple shear flow. In this sense, we may argue that the effects of Re and Da on viscosities in 2D and 3D cases are qualitatively similar, but quantitatively different. However, this needs further investigations. For $10^{-6} \le Da \le 10^{-4}$, the curves of intrinsic viscosity vs Re nearly overlap with each other. Whereas for $10^{-3} \le Da \le 10^{-1}$, the intrinsic viscosity decreases quickly with Da at various Re, as can be seen in Figs. 14(a)–14(d). We have proposed an empirical formula to correlate the intrinsic viscosity with Da at sufficiently low Re where the fluid inertia can be completely neglected,[30]

$$< \tilde{\eta} > = \frac{m}{1 + n \times Da^{2/3}}. \tag{23}$$

In Eq. (23), m is the intrinsic viscosity of suspensions containing the corresponding solid particle and n is a fitting parameter. For finite Re where the fluid inertia plays an important role, we found that the relation between the intrinsic viscosity and Da can be described by Eq. (23) as well. The parameters m and n at different Re are listed in Table V. The parameter m, which can be obtained by setting the Da to be extremely small ($Da = 10^{-12}$), increases linearly with Re. The parameter n seems to be a constant at different Re, especially for $Re \ge 5$.

V. CONCLUSIONS

In this work, we studied the rotation of an elliptical porous particle in a simple shear flow and the associated shear viscosity by solving the volume-averaged macroscopic equations using a 2D lattice Boltzmann model, focusing on the effects of the fluid inertia and the permeability of the particle. Our model was first validated by examining the torque on the elliptical porous particle exerted by the fluid in a simple shear flow at sufficiently low Re and the rotational behaviors of solid impermeable elliptical particles for Re up to 30, including the angular rate and rotation period. All the results were compared to analytical solutions and simulation results available in the literature.

First, we studied the effects of permeability and fluid inertia on the rotational behaviors of elliptical porous particles. Results demonstrate that for elliptical porous particles with small and intermediate Da ranging from 10^{-6} to 2×10^{-2}, there is a critical Reynolds number Re_c at which the particle would transit from rotary to stationary. These porous particles rotate in a time-periodic mode with a non-uniform angular rate in a simple shear flow with $Re < Re_c$. The rotation period increases rapidly to infinity when Re increases to Re_c, whereas the maximum and minimum angular rates decrease with Re. This may be attributed to the increase in negative torque exerted on the particle owing to the enhanced fluid inertia. Particularly, for particles with small $Da = 10^{-6}$–10^{-3}, the permeability has a minor effect on the rotational behaviors of porous particles. Besides, we have extended the scaling law,[12] which is initially proposed for solid impermeable elliptical particles, to the corresponding porous ones with $Da = 10^{-6}$–2×10^{-2} to describe the relation between the rotation period and Re with the fitting parameters C and Re_c dependent on Da. The Re_c remains constant for $Da = 10^{-6}$–10^{4} and increases with the increase in Da for $Da = 10^{-3}$–2×10^{-2}. For highly permeable elliptical particles with $Da = 2 \times 10^{-2}$–10^{-1}, the rotation periods are smaller than those of smaller Da and the minimum angular rates are bigger than those of smaller Da. This may be attributed to the decrease in negative torque due to the higher permeability. The rotation period increases slowly and nonlinearly with Re, and the minimum angular rate decreases with Re similarly. By extrapolation, there may exist a critical Reynolds number for highly permeable particles at which these particles would stop rotating, but this conclusion needs further validation. The maximum angular rate decreases with the increase in Re where the permeability plays an unimportant role.

We also checked the shear viscosity of suspensions including an elliptical porous particle in a simple shear flow. Results show that the relative viscosity increases with enhanced fluid inertia, meaning that the suspensions are shear-thickening. A reduction of relative viscosity was found when Da increases, while the intrinsic viscosity shows a linear increase with Re. An empirical formula initially proposed for vanishing Re can be extended to correlate the intrinsic viscosity with Da at finite Re. These results for the rotation of an elliptical porous particle in shear flow are favorable in the fundamental understanding of the complicated particulate two-phase flows containing porous particles that are of wide interest in a variety of industrial and natural processes. As the first step toward our ambition to understanding the effects of fluid inertia and permeability on the rotation of porous particles, we begin our research with 2D cases. The reasons are twofold. First, 2D simulation results, although being greatly simplified, can well reflect the physical mechanisms underlying the fluid–particle interaction with varying fluid inertia and permeability. Second, 2D simulations are computationally much cheaper than 3D simulations for the same fluid–particle configuration. It is our long term target to develop 3D LBM model based on the volume-averaged macroscopic equations[26] and optical imaging methods[47] to gain the complete picture of the interaction between fluid flow and moving porous particles.

ACKNOWLEDGMENTS

This work was subsidized by the National Natural Science Foundation of China (Grant No. 91834302).

REFERENCES

[1]D. W. Qi and L.-S. Luo, "Rotational and orientational behaviour of three-dimensional spheroidal particles in Couette flows," J. Fluid Mech. **477**, 201 (2003).
[2]J. J. Stickel and R. L. Powell, "Fluid mechanics and rheology of dense suspensions," Annu. Rev. Fluid Mech. **37**, 129 (2005).
[3]S. Blaser, "Flocs in shear and strain flows," J. Colloid Interface Sci. **225**, 273 (2000).
[4]P. Tian, Y. Wei, M. Ye, and Z. Liu, "Methanol to olefins (MTO): From fundamentals to commercialization," ACS Catal. **5**, 1922 (2015).
[5]M.-Y. Ma, Y.-J. Zhu, L. Li, and S.-W. Cao, "Nanostructured porous hollow ellipsoidal capsules of hydroxyapatite and calcium silicate: Preparation and application in drug delivery," J. Mater. Chem. **18**, 2722 (2008).
[6]G. B. Jeffery, "The motion of ellipsoidal particles immersed in a viscous fluid," Proc. R. Soc. London, Ser. A **102**, 161 (1922).
[7]C. R. Robertson and A. Acrivos, "Low Reynolds number shear flow past a rotating circular cylinder. Part 1. Momentum transfer," J. Fluid Mech. **40**, 685 (1970).
[8]E. Y. Harper and I.-D. Chang, "Maximum dissipation resulting from lift in a slow viscous shear flow," J. Fluid Mech. **33**, 209 (1968).
[9]L. G. Leal, "The slow motion of slender rod-like particles in a second-order fluid," J. Fluid Mech. **69**, 305 (1975).
[10]J. Einarsson, F. Candelier, F. Lundell, J. R. Angilella, and B. Mehlig, "Rotation of a spheroid in a simple shear at small Reynolds number," Phys. Fluids **27**, 063301 (2015).
[11]J. Feng and D. D. Joseph, "The unsteady motion of solid bodies in creeping flows," J. Fluid Mech. **303**, 83 (1995).
[12]E.-J. Ding and C. K. Aidun, "The dynamics and scaling law for particles suspended in shear flow with inertia," J. Fluid Mech. **423**, 317 (2000).
[13]C. M. Zettner and M. Yoda, "Moderate-aspect-ratio elliptical cylinders in simple shear with inertia," J. Fluid Mech. **442**, 241 (2001).
[14]Z. Yu, N. Phan-Thien, and R. I. Tanner, "Rotation of a spheroid in a Couette flow at moderate Reynolds numbers," Phys. Rev. E **76**, 206310 (2007).
[15]H. Huang, X. Yang, M. Krafczyk, and X.-Y. Lu, "Rotation of spheroidal particles in Couette flows," J. Fluid Mech. **692**, 369 (2012).
[16]H. Huang, Y. Wu, and X. Lu, "Shear viscosity of dilute suspensions of ellipsoidal particles with a lattice Boltzmann method," Phys. Rev. E **86**, 046305 (2012).
[17]W. Mao and A. Alexeev, "Motion of spheroid particles in shear flow with inertia," J. Fluid Mech. **749**, 145 (2014).
[18]S.-L. Huang, S.-D. Chen, T.-W. Pan, C.-C. Chang, and C.-C. Chu, "The motion of a neutrally buoyant particle of an elliptic shape in two dimensional shear flow: A numerical study," Phys. Fluids **27**, 083303 (2015).
[19]R.-Y. Li, Z.-W. Cui, W.-X. Huang, L.-H. Zhao, and C.-X. Xu, "On rotational dynamics of a finite-sized ellipsoidal particle in shear flows," Acta Mech. **230**, 449 (2019).
[20]H. Masoud, H. A. Stone, and M. J. Shelley, "On the rotation of porous ellipsoids in simple shear flows," J. Fluid Mech. **733**, R6 (2013).
[21]G. Neale, N. Epstein, and W. Nader, "Creeping flow relative to permeable spheres," Chem. Eng. Sci. **28**, 1865 (1973).
[22]A. C. Michalopoulou, V. N. Burganos, and A. C. Payatakes, "Hydrodynamic interactions of two permeable particles moving slowly along their centerline," Chem. Eng. Sci. **48**, 2889 (1993).
[23]B. C. Roy and E. R. Damiano, "On the motion of a porous sphere in a Stokes flow parallel to a planar confining boundary," J. Fluid Mech. **606**, 75 (2008).
[24]M. P. Dalwadi, S. J. Chapman, S. L. Waters, and J. M. Oliver, "On the boundary layer structure near a highly permeable porous interface," J. Fluid Mech. **798**, 88 (2016).
[25]Z. Guo and T. S. Zhao, "Lattice Boltzmann model for incompressible flows through porous media," Phys. Rev. E **66**, 036304 (2002).
[26]L. Wang, L.-P. Wang, Z. Guo, and J. Mi, "Volume-averaged macroscopic equation for fluid flow in moving porous media," Int. J. Heat Mass Transfer **82**, 357 (2015).
[27]C. Li, M. Ye, and Z. Liu, "On the rotation of a circular porous particle in 2D simple shear flow with fluid inertia," J. Fluid Mech. **808**, R3 (2016).
[28]A. Xu, L. Shi, and T. S. Zhao, "Lattice Boltzmann simulation of shear viscosity of suspensions containing porous particles," Int. J. Heat Mass Transfer **116**, 969 (2018).
[29]X. Liu, H. Huang, and X.-Y. Lu, "Lattice Boltzmann study of effective viscosities of porous particle suspensions," Comput. Fluids **181**, 135 (2019).
[30]J. Liu, C. Li, M. Ye, and Z. Liu, "On the shear viscosity of dilute suspension containing elliptical porous particles at low Reynolds number," Powder Technol. **354**, 108 (2019).
[31]T. Rezaee and K. Sadeghy, "Effect of porosity on the settling behavior of a 2D elliptic particle in a narrow vessel: A lattice-Boltzmann simulation," Phys. Fluids **31**, 123301 (2019).
[32]C. K. Aidun, Y. Lu, and E.-J. Ding, "Direct analysis of particulate suspensions with inertia using the discrete Boltzmann equation," J. Fluid Mech. **373**, 287 (1998).
[33]S. Ergun, "Fluid flow through packed columns," Chem. Eng. Prog. **48**, 89 (1952).
[34]S. Bhattacharyya, S. Dhinakaran, and A. Khalili, "Fluid motion around and through a porous cylinder," Chem. Eng. Sci. **61**, 4451 (2006).
[35]J. C. Ladd, "Numerical simulations of particulate suspensions via a discretized Boltzmann equation. Part 2. Numerical results," J. Fluid Mech. **271**, 311 (1993).
[36]Z.-G. Feng and E. E. Michaelides, "The immersed boundary-lattice Boltzmann method for solving fluid-particles interaction problems," J. Comput. Phys. **195**, 602 (2004).
[37]Q. Zou and X. He, "On pressure and velocity boundary conditions for the lattice Boltzmann BGK model," Phys. Fluids **9**, 1591 (1997).
[38]R. Mei, D. Yu, W. Shyy, and L.-S. Luo, "Force evaluation in the lattice Boltzmann method involving curved geometry," Phys. Rev. E **65**, 041203 (2002).
[39]T. Rosén, F. Lundell, and C. K. Aidun, "Effect of fluid inertia on the dynamics and scaling of neutrally buoyant particles in shear flow," J. Fluid Mech. **738**, 563 (2014).
[40]A. Einstein, "Eine neue bestimmung der Moleküldimensionen," Ann. Phys. **324**, 289 (1906).
[41]J. F. Brady, "The Einstein viscosity correction in n dimensions," Int. J. Multiphase Flow **10**, 113 (1984).
[42]I. M. Krieger and T. J. Dougherty, "A mechanism for non-Newtonian flow in suspensions of rigid spheres," Trans. Soc. Rheol. **3**, 137 (1959).
[43]W. H. Graf, *Hydraulics of Sediment Transport* (McGraw-Hill, New York, 1971).
[44]Z. Zhu, H. Wang, and D. Peng, "Dependence of sediment suspension viscosity on solid concentration: A simple general equation," Water **9**, 474 (2017).
[45]S. Yamamoto and T. Matsuoka, "Viscosity of dilute suspensions of rod-like particles: A numerical simulation method," J. Chem. Phys. **100**, 3317 (1994).
[46]C.-J. Lin, J. H. Peery, and W. R. Schowalter, "Simple shear flow round a rigid sphere: Inertial effects and suspension rheology," J. Fluid Mech. **44**, 1 (1970).
[47]L. Ma, S. Xu, X. Li, Q. Guo, D. Gao, Y. Ding, M. Ye, and Z. Liu, "Particle tracking velocimetry of porous sphere settling under gravity: Preparation of the model porous particle and measurement of drag coefficients," Powder Technol. **360**, 241 (2020).